Atmospheric Research 99 (2011) 290–301

Contents lists available at ScienceDirect

Atmospheric Research

journal homepage: www.elsevier.com/locate/atmos

Droplet growth in a bin warm-rain scheme with Twomey CCN activation

Wojciech W. Grabowski [a,*], Miroslaw Andrejczuk [b], Lian-Ping Wang [c]

[a] National Center for Atmospheric Research, Boulder, Colorado, USA
[b] University of Leeds, Leeds, United Kingdom
[c] University of Delaware, Newark, Delaware, USA

ARTICLE INFO

Article history:
Received 30 October 2009
Received in revised form 12 July 2010
Accepted 20 October 2010

Keywords:
Cloud physics
Bin microphysics;
Droplet activation
Warm-rain processes

ABSTRACT

This paper discusses improvements to the bin warm-rain microphysics scheme that applies the Twomey approach to represent CCN activation. The Twomey approach relates the concentration of activated droplets to the maximum supersaturation experienced by the air parcel during activation and thus avoids complications of CCN size distribution and chemical composition that are considered in more complicated activation schemes. When using the traditional Twomey scheme, activated droplets are typically inserted into the first bin of the bin microphysics scheme. As shown in our previous study, this does not allow numerical convergence when the number of bins is increased. In addition, CCN characteristics are important for early growth of cloud droplets and it is unclear if an approach where such characteristics are not considered provides a valid strategy for modeling diffusional growth of small cloud droplets. We included relatively simple modifications to the bin warm-rain microphysics with Twomey approach to CCN activation and apply the improved scheme to idealized Lagrangian parcel simulations as well as 1D Eulerian updraft simulations. We compare results of the improved scheme with the benchmark results from a sophisticated aerosol activation and growth model. Two observationally-based aerosol characteristics are employed in the comparison, the pristine from DYCOMS and polluted from VOCALS. The results suggest that the improved bin scheme compares relatively well with the benchmark, and leads to numerical results that are significantly less sensitive to the number of bins applied. The results also suggest the minimum bin and spatial resolutions that need to be used in the large-eddy simulation to investigate with confidence the impact of cloud turbulence on warm-rain development.

1. Introduction

Modeling microphysical processes in warm ice-free clouds involves representation of cloud droplet activation and their growth by the diffusion of water vapor and by collision/coalescence. These are commonly referred to as warm-rain processes and are typically modeled using the continuous medium approach, where the condensed water is represented by a set of field variables, such as mixing ratios, number concentrations, etc. Among such modeling techniques, the detailed (or bin) microphysics is the most comprehensive because the spectrum of cloud droplets and drizzle/rain drops is represented using a finite number of size classes (e.g., Clark 1973; Feingold et al., 1988, 1994; Kogan 1991; Ackerman et al. 1995; Khain et al. 2004). For that, the spectral density function $f(r) \equiv dn(r)/dr$ is used, where $n(r)$ is the concentration, per unit mass of dry air, of drops smaller than r (i.e., the cumulative number concentration). In this approach, activation of cloud condensation nuclei (CCN) provides a source of cloud droplets at the small-size-end of the spectral representation and subsequent growth of cloud droplets shifts the spectral density function toward larger sizes.

* Corresponding author. NCAR/MMM, P.O. Box 3000, Boulder, CO 80307-3000, USA.
E-mail address: grabow@ucar.edu (W.W. Grabowski).

0169-8095/$ – see front matter © 2010 Elsevier B.V. All rights reserved.
doi:10.1016/j.atmosres.2010.10.020

This paper concerns representation of warm-rain processes in bin warm-rain microphysics schemes that relate the number of activated droplets to the maximum supersaturation experienced during activation. Such a relationship is typically referred to as the Twomey relationship and it is often expressed as:

$$N_{CCN} = C_0(100S)^k \quad (1)$$

where N_{CCN} is the concentration of activated CCN at the supersaturation S, and C_0 and k are coefficients based on the observed characteristics of the CCN (Twomey 1959; see also Pruppacher and Klett 1997). In some studies, different coefficients C_0 and k are used for low and high values of S (e.g., $k=4$ for $S<0.1\%$ and $k=0.4$ for $S\geq 0.1\%$) and an upper limit of activated CCN is imposed [e.g., (1) and (2) in Rasmussen et al. 2002]. One can also use a tabulated $N_{CCN}-S$ relationship instead of an analytic expression (1), an approach used in this paper. We will refer to a bin microphysics scheme applying Eq. (1) to represent CCN activation as the Twomey bin microphysics scheme.

In a traditional numerical implementation of Eq. (1), activation of cloud droplets proceeds in the following way. At every time step, the value of the predicted supersaturation S is compared to the maximum supersaturation S_{max} experienced by the parcel in the past.[1] If $S>S_{max}$, additional CCN have to be activated and their number is derived as $\Delta n = C_0 (100S)^k - C_0 (100S_{max})^k$ (if specified, the upper limit of activated CCN has to be observed when deriving Δn). Subsequently, the spectral density function in the first bin is increased by $\Delta n/\Delta r^{(1)}$ ($\Delta r^{(1)}$ is the width of the first radius bin) and S_{max} takes the value of S. Such a simple approach, used in the past in Twomey bin warm-rain microphysics schemes (e.g., Clark 1974; Hall 1980; Grabowski 1989; Stevens et al. 1996; Rasmussen et al. 2002) leads to realistic predictions of the droplet concentration, but not necessary spectral characteristics after activation (see Grabowski and Wang 2009—hereinafter GW09—for a detailed discussion). In some approaches, activated CCN are assumed to follow a prescribed distribution which is used to distribute newly activated droplets on the bin grid (e.g., Reisin et al. 1996).

An important computational advantage of the Twomey approach is that only "bulk" properties of the CCN are considered, and the details of the CCN size distribution and chemical composition are excluded. However, the chemical composition (together with kinetic and curvature effects) impacts the growth of cloud droplets after activation, typically until they reach the radius of several microns. Inserting activated droplets into the first radius bin only is not realistic either and does not allow numerical convergence of the entire bin scheme when the number of bins is increased (cf. GW09). In general, the outcome of the CCN activation scheme depends not only on how many CCN become activated and on where (on the bin grid) to insert the activated CCN, but also on how small droplets grow after activation. This is because the peak supersaturation [that according to Eq. (1) sets the total number of activated droplets] is determined by the balance of the supersaturation source (e.g., the cloud updraft) and the supersaturation sink (water vapor absorption on growing droplets and the latent heat release). The peak supersaturation is reached when the two exactly balance each other. It follows that the activation in the bin scheme also requires an adequate prediction of the growth of already activated droplets where kinetic, curvature and solute effects are all important. The kinetic and curvature effects can be easily included, but the solute effect is more difficult to treat because the Twomey bin scheme does not carry the solute information.

It thus seems that applying the Twomey relationship (1) in a bin scheme may not be justified and a more sophisticated technique is required. Possible approaches include the two-dimensional bin scheme (i.e., applying a discrete number of aerosol size bins for each droplet size; e.g., Bott 2000, Simmel and Wurzler 2006) or a hybrid technique in which growth of haze particles (i.e., solution droplets prior to activation) is treated separately from the growth of activated cloud droplets (e.g., Kogan 1991, Ackerman et al. 1995, Leroy et al. 2007; see the review in Khain et al. 2000). The overall goal of the investigation reported in this paper is to explore this issue in more detail. The specific motivation comes from GW09, where a Twomey bin microphysics scheme was applied in the rising adiabatic parcel framework to investigate the impact of turbulent enhancement of droplet collisions on the warm-rain development. GW09 attempted to obtain converged numerical solutions to the rain development in the rising adiabatic parcel framework. The latter proved difficult, arguably because of the simplifications of the activation scheme and the representation of the diffusional growth of small cloud droplets. The current paper documents modifications of the Twomey bin scheme and applies an accurate Lagrangian aerosol growth model as a benchmark for droplet activation and their diffusional growth.

The next section presents the Lagrangian benchmark model. The model traces growth of 10,000 solution droplets randomly selected from the assumed initial CCN size distribution with prescribed chemical composition. Section 3 details modifications of the Eulerian bin scheme, including representation of the activation using the Twomey formula (1). Results from the Lagrangian benchmark model are used as reference for the Lagrangian (time evolution) and 1D Eulerian (time-and-height-evolution) models applying the bin approach outlined in this paper. These are presented in Section 4 and contrasted with the approach used in GW09. Simulations reported in GW09 are revisited using the modified bin scheme in Section 5. A brief summary in Section 6 concludes the paper.

2. Activation and early growth of cloud droplets: the benchmark model

The equation describing the rate of growth of a small cloud droplet with radius r and containing a dissolved salt forms the basis for the benchmark model of the CCN activation and early growth of cloud droplets. This equation can be approximated by (e.g., Howell 1949; Fukuta and Walter 1970; Kogan 1991; Pruppacher and Klett 1997):

$$\frac{dr}{dt} = \frac{G}{r}\left(S - S_{eq}\right) \quad (2)$$

[1] In multidimensional Eulerian cloud models, the number of activated CCN is one of the model variables (e.g., Eq. (7) in Morrison and Grabowski 2008). This provides the same information as S_{max}.

where $S=e/e_s-1$ is the supersaturation (e and e_s are the water vapor pressure and its saturated value, respectively), $S_{eq}=\exp(A/r-B/r^3)-1\approx A/r-B/r^3$ is the equilibrium supersaturation (where A depends on the surface tension and temperature, and represents the Kelvin or curvature effect; and B depends on the solute properties and represents the Raoult or solution effect; Pruppacher and Klett 1997, Section 6.5), and

$$G=\left[\frac{\rho_w R_v T}{e_s D}+\frac{\rho_w L}{KT}\left(\frac{L}{R_v T}-1\right)\right]^{-1}, \tag{3}$$

where ρ_w is the density of water, R_v is the water vapor gas constant, T is the temperature, D is the diffusivity of water vapor in the air, L is the latent heat of condensation, and K is the thermal conductivity of air. Note that D and K need to include kinetic effects (i.e., the effects of condensation and accommodation coefficients; e.g., Fukuta and Walter 1970).

To use Eq. (2) in the representation of droplet activation and early growth requires the information about the chemical composition and size distribution of the CCN. This is why Eq. (2) is typically used in models that trace the Lagrangian evolution of a set of aerosol dry masses. The benchmark model used here is of that type: it traces the evolution of 10,000 aerosol particles randomly selected from the assumed aerosol size distribution and is based on the Lagrangian microphysics model described in Andrejczuk et al. (2008). The initial conditions for the benchmark model assume equilibrium size at water saturation. Details of the benchmark model are given in the Appendix.

Two aerosol populations are used, both based on actual field observations: the DYCOMS case corresponds to the pristine environment (e.g., Ackerman and Coauthors, 2009) and the VOCALS case represents a polluted environment (the specific data come from observations between 11.14 and 11.47 UTC of the flight B420 of the UK research plane BAe-146). Fig. 1 shows the concentration of activated droplets N_{CCN} versus the supersaturation S for the two aerosol populations. The N_{CCN} versus S relationships are obtained using the benchmark model by exposing aerosols to the constant supersaturation S and allowing sufficient time to partition the aerosol population into unactivated haze particles and activated (and growing) cloud droplets. Concentration of the latter is taken as N_{CCN}. The figure highlights the differences between the pristine and polluted conditions, with the polluted VOCALS aerosols reaching the maximum activated droplet concentration of about 540 mg^{-1} for $S\approx 1\%$ and pristine DYCOMS aerosols saturating at 190 mg^{-1} for $S\approx 4\%$. Note that the relationships shown in Fig. 1 correspond to the analytic Twomey relationship (1) and their tabulated forms are used in the bin microphysics scheme used in this paper.

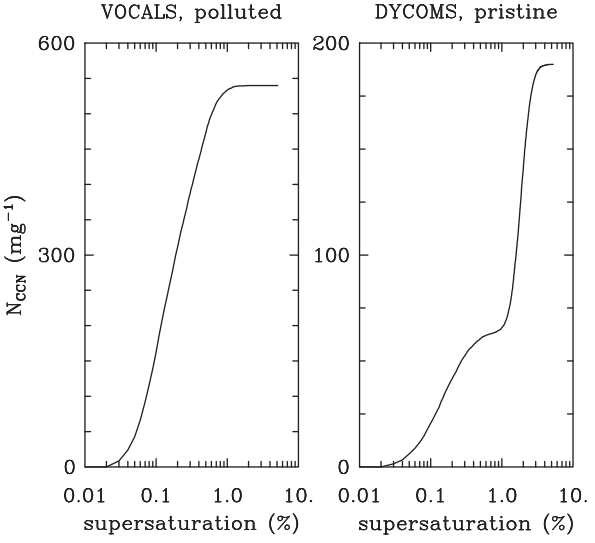

Fig. 1. Cumulative number of activated CCN versus the supersaturation for the two aerosol conditions applied.

3. A simplified approach for an Eulerian bin scheme with Twomey CCN activation

The Eulerian bin warm-rain microphysics scheme applied here is similar to that used in Morrison and Grabowski (2007), GW09, and Grabowski et al. (2010). The analytic equation for the spectral density function for the case of droplet activation and diffusional growth only and neglecting droplet sedimentation is:

$$\frac{\partial f}{\partial t}+\frac{1}{\rho_o}\nabla\cdot(\rho_o \mathbf{u} f)+\frac{\partial}{\partial r}\left(\frac{dr}{dt}f\right)=\left(\frac{\partial f}{\partial t}\right)_{act}, \tag{4}$$

where $\mathbf{u}$ is the fluid flow velocity and $\rho_o(z)$ is the anelastic base state air density. The third term on the left-hand-side represents growth of cloud droplets by the condensation of water vapor (or their evaporation in subsaturated air) which are represented by the advection of f in the radius space, with dr/dt being the rate of change of the droplet/drop radius r due to condensation or evaporation. The term of the rhs represents the cloud droplet activation (i.e., the initial source of cloud droplets). In the discrete system consisting of N bins (or classes) of drop sizes, the spectral density function for each bin (i) is defined as $f^{(i)}=n^{(i)}/\Delta r^{(i)}$, where $n^{(i)}$ is the concentration (per unit mass of dry air) of drops in the bin i, $\Delta r^{(i)}=r^{(i+1)}-r^{(i)}$ is the width of the bin, and bin boundaries $r^{(i)}$ ($i=1,N+1$) are prescribed as discussed later in the paper (cf. Section 3.3). This transforms the continuous Eq. (4) into a system of N coupled equations (e.g., Morrison and Grabowski 2007):

$$\frac{\partial f^{(i)}}{\partial t}+\frac{1}{\rho_o}\nabla\cdot\left(\rho_o \mathbf{u} f^{(i)}\right)=\left(\frac{\partial f^{(i)}}{\partial t}\right)_{cond}+\left(\frac{\partial f^{(i)}}{\partial t}\right)_{act} \quad \text{for } i=1,\ldots,N, \tag{5}$$

where the first term on the rhs represents the condensation/evaporation of cloud droplets (i.e., the transport of droplets across the bin space) and, as in Eq. (4), the second term represents cloud droplet activation.

The modifications of the bin scheme applied in GW09 include a revised activation scheme as well as the analytic form and numerical representation of the diffusional growth of cloud droplets. These are detailed below.

3.1. The improved activation scheme

As explained above, representation of droplet activation with the Twomey $N_{CCN}-S$ relationship typically involves

adding activated droplets to the first radius bin (typically the radius of around 1 μm). As documented in GW09, such an approach is ill-posed from the numerical point of view when the number of bins is changed. A sensible modification is to insert activated droplets into bins that their activation radius r_{act} (also referred to as the critical radius; cf. Pruppacher and Klett 1997; Section 6.5) falls into. Assuming that haze particles rapidly approach their quasi-equilibrium size, r_{act} can be related to the activation supersaturation S_{act}, that is, the maximum of the equilibrium supersaturation S_{eq} in Eq. (2). Since $S_{act}=(4A^3/27B)^{1/2}$ and $r_{act}=(3B/A)^{1/2}$, it follows that (e.g., Khain et al. 2000 and references therein; Leroy et al. 2007):

$$S_{act} = \frac{2A}{3\, r_{act}}. \tag{6}$$

A notable feature of Eq. (6) is that it is independent of the solute characteristics (A depends on the water surface tension and temperature only) and thus can be used independently of CCN characteristics. In the numerical implementation, activated droplets can then be inserted into progressively smaller and smaller bins when the supersaturation increases near the cloud base, with the total number of activated droplets N_{act} given by the Twomey relationship. A graph of Eq. (6) for $T=288.16$ K is shown in Fig. 2. For typical values of S, say, between 0.1 and 1.0%, the activation radii r_{act} are between a fraction of 0.1 μm and 1 μm. It follows that (unlike in GW09) the bin grid should extend below 1 μm; otherwise, most of the activated droplets will end up in the first radius bin anyway. Another important factor is that when S is just slightly above saturation (say, around 0.01%), Eq. (6) implies that relatively large bins have to be filled with activated droplets.[2] However, the low values of S_{act} correspond to large CCN that reach their quasi-equilibrium size relatively slowly. It follows that the modified activation scheme should prescribe the maximum bin size from which the activation starts; in the implementation used here the maximum radius is selected as 2 μm.

3.2. Droplet diffusional growth and its representation in the bin scheme

The growth rate of cloud droplets applied in Eqs. (4) and (5) is a simplified form of Eq. (2), neglecting the curvature and solute effects but including the kinetic effects, namely

$$\frac{dr}{dt} = \frac{G'}{r + r_0} S, \tag{7}$$

where G' is similar to G in Eq. (3) but with the diffusivity of water vapor D' and air thermal conductivity K' excluding the kinetic effects. The kinetic effects are now included through the parameter r_0 (e.g., Clark, 1974; Eq. 2.18 in Kogan, 1991).

[2] Note that the concentration of these large CCN is small and they affect insignificantly activation of smaller CCN. However, if present, these large CCN, especially giant and ultra-giant, are important for drizzle/rain formation. A different strategy needs to be developed to include giant and ultra-giant CCN into the Twomey activation scheme, an aspect not considered here.

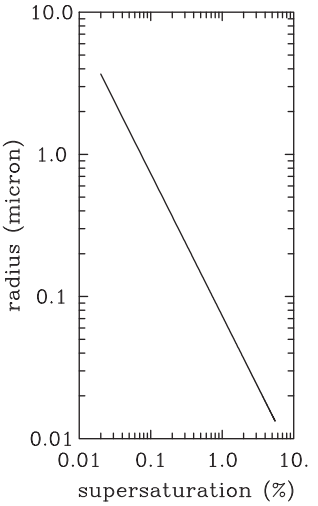

Fig. 2. Activation (critical) radius versus the activation (critical) supersaturation as given by (6) for $T=288.16$ K.

For the conditions used in the tests presented in the subsequent sections, constant values of $G'=9.152\times 10^{-11}$ m^2 s^{-1} and $r_0=1.86$ μm are used (the latter is derived assuming condensation coefficient of 0.036, i.e., as in the benchmark model). Note that GW09 excluded the kinetic effects (i.e., $r_0=0$). Note also that Clark (1974), Srivastava (1991) and Kogan(1991) included the surface tension term into Eq. (7); that is, they used $S-A/r$ instead of S on rhs of Eq. (7). We do not think this is appropriate because such an approach can result in an oscillatory behavior of the bin scheme during the activation phase. This is because some of the activated small droplets will evaporate if $S-A/r<0$ only to be activated back to maintain N_{act} in agreement with the actual value of S.

In our previous studies (e.g., Grabowski 1989, Morrison and Grabowski 2007, GW09) condensation/evaporation of cloud droplets as well as evaporation of drizzle/rain drops was calculated using the 1D MPDATA advection scheme of Smolarkiewicz (1984). Here, we apply an approach already applied in Grabowski et al. (2010) that combines the analytic Lagrangian solution of the condensational growth with remapping of the spectral distribution onto the original radius grid using piecewise linear functions. Overall, this technique is similar to that used by Simmel and Wurzler (2006; Section 3.1.2 and references therein); see appendix in Grabowski et al. (2010) for further details. This modification is important for the extension of the bin grid toward sub-micron sizes because the time step is not limited by the stability criteria of the 1D Eulerian flux-form advection.

3.3. Grid for the bin scheme

Following the approach used in GW09, we will use two bin resolutions by applying two different numbers of bins N: 112 and 300. As in previous studies, we apply a linear-mass doubling grid which combines the linear grid with a grid often used in collision/coalescence studies where the drop

mass doubles every s bins. The radius r_i (in μm) defining the bin boundary is obtained as:

$$r_i = (i-1)\alpha + \left(\frac{3m_i}{4\pi\rho_w}\right)^{1/3} \text{for } i = 1,\ldots,N+1, \quad (8)$$

where the mass m_i is given by the recurrence $m_i/m_{i-1} = 2^{1/s}$ and m_0 is taken as the mass of a droplet with 1-μm radius [the second term on rhs of Eq. (8) needs to be converted into microns before it is added to the first term]. With $N=112$ we use $\alpha=0.2$ μm and $s=3$; $\alpha=0.125$ μm and $s=8$ is used with $N=300$. Note that $r_1=1$ μm for both values of N. The modified grid r'_i (in μm) is defined as:

$$r'_i = r_i - 1 \text{ μm}, \quad (9)$$

which implies that $r'_1=0$. The four grid configurations are shown in Fig. 3.

The $N=300$ case corresponds to almost-converged solutions for the rain development (i.e., increasing further the number of bins leads to insignificant changes in the results). The $N=112$ represents the bin setup that we plan to use in large-eddy simulations of shallow convection. The key point is that with all modifications described in this paper, the $N=112$ setup results in numerical solutions relatively close to the converged solutions as well. The above statements are supported by results discussed in Section 5 using two additional bin scheme setups, $N=400$ (with $\alpha=0.125$ μm and $s=10$) and $N=72$ (with $\alpha=0.25$ μm and $s=1.9$).

4. Comparison between the benchmark and the bin scheme

In this section, we apply developments discussed above to two sets of tests for which the Lagrangian aerosol activation and growth model from Section 2 serves as a benchmark (hereinafter referred to BNCHMK). In the first set of tests, we apply the bin scheme in the Lagrangian parcel framework, exactly as used in BNCHMK, to compare details of the activated droplet spectra. The emphasis in these tests is on the performance of the improved scheme when compared to GW09, and on the impact of bin grid resolution when compared to BNCHMK. In the second set of tests, the improved bin scheme is used in 1D Eulerian framework, where additional complications of the spatial discretization are considered (i.e., the numerical solution is affected not only by the time truncation errors, but the spatial truncation errors as well). Such a strategy follows tests reported in Clark (1974) and Morrison and Grabowski (2008).

Simulations applying the Eulerian bin scheme which includes all the developments reported above will be referred to as NEW. NEW simulations include the improved activation scheme, modified diffusional growth formulation (6), and the bin grid as given by Eq. (9). These simulations will be contrasted with simulations OLD applying the setup similar to GW09: the activation scheme which inserts activated droplets into the first radius bin, diffusional growth equation without kinetic effects, and bin grid as given by Eq. (8). To show that all the modifications included into NEW setup play role in the improvements, we also show some results from tests where the OLD setup is used with kinetic effects, i.e., using Eq. (6) with OLD activation and bin grid. These simulations will be referred to as OLD-KIN. Note that NEW, OLD, and OLD-KIN all include the new numerical representation of diffusional growth (Section 3.2). The results shown here represent a fraction of simulations applying various combinations of differences between NEW and OLD schemes and different bin resolutions that were performed in the course of this study.

In all tests we apply aerosol characteristics presented in Fig. 1 (referring to them as pristine and polluted) and three values of the vertical velocity: 0.2, 1 and 5 m s^{-1}. For the adiabatic parcel calculations, the starting level temperature and pressure are 288.16 K and 900 hPa, respectively, and the relative humidity of 100%. The time steps applied in the bin model vary depending on the updraft speed and N. Typical values range between 0.005/0.02 s for $N=300$ and updraft of 5/0.2 m s^{-1} to 0.05/0.2 s for $N=112$ and updraft of 5/0.2 m s^{-1}.

4.1. Rising-parcel calculations

For reference, Figs. 4 and 5 show results from the BNCHMK simulations for the polluted and pristine aerosol, respectively. Note that the logarithmic scale is used on the vertical distance axis to better expose activation phase. In BNCHMK, first droplets are activated at a distance between about 4 m (for

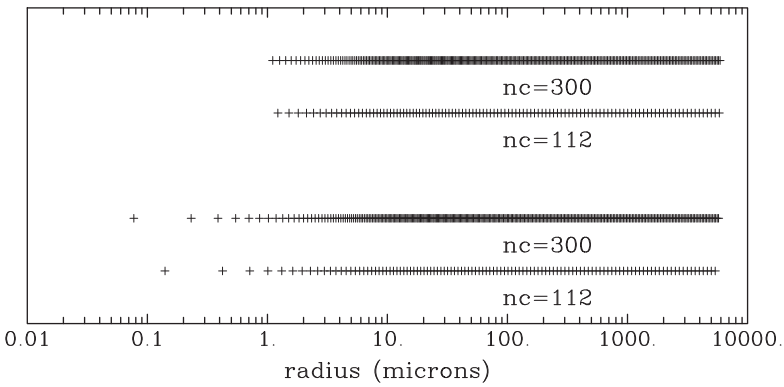

Fig. 3. Grids used in the simulations described in this paper. The upper two grids starting at 1 μm correspond to Eq. (8) and were used in GW09. Bottom two are given by Eq. (9) and they start at 0 μm. Each plus sign represents the bin center.

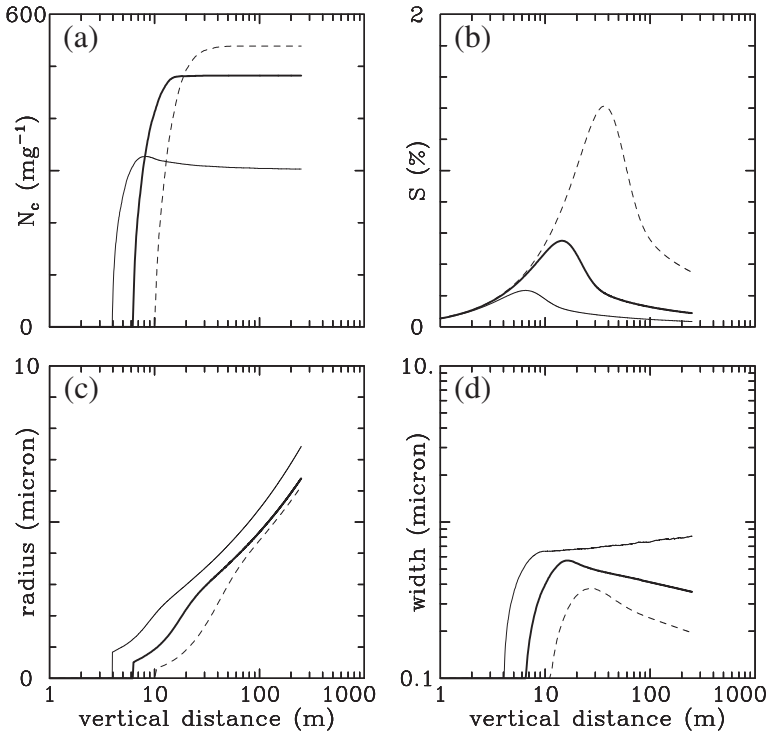

Fig. 4. Results from the benchmark Lagrangian aerosol growth model (Section 2) for the polluted aerosols from VOCALS campaign. The panels show (a) the concentration of activated droplets, (b) supersaturation, (c) mean radius, and (d) spectral width versus height above the $S=0$ level. The thin solid, thick solid, and dashed lines are for parcel vertical velocity of 0.2, 1.0 and 5.0 m s^{-1}, respectively.

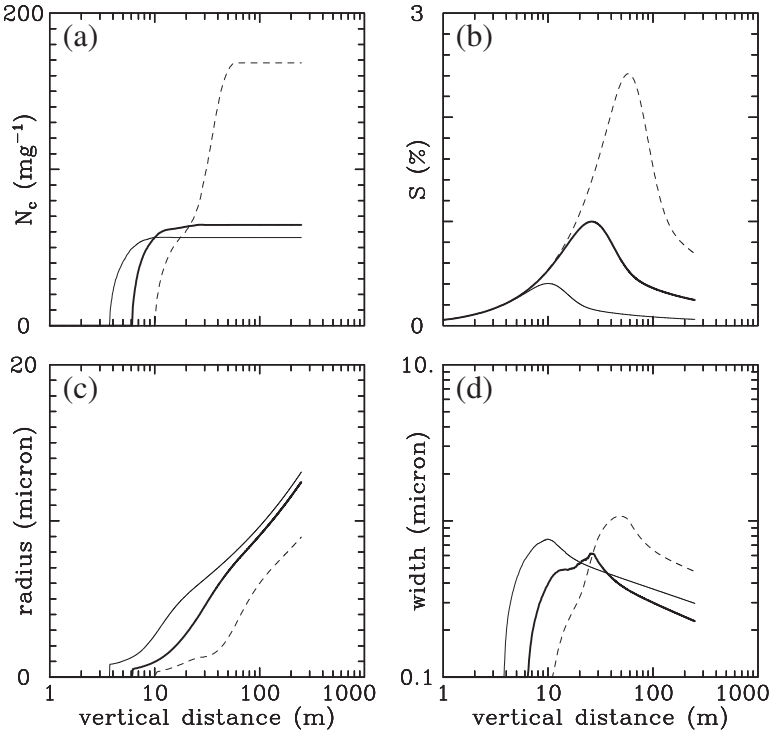

Fig. 5. As Fig. 4, but for the pristine aerosol from DYCOMS campaign.

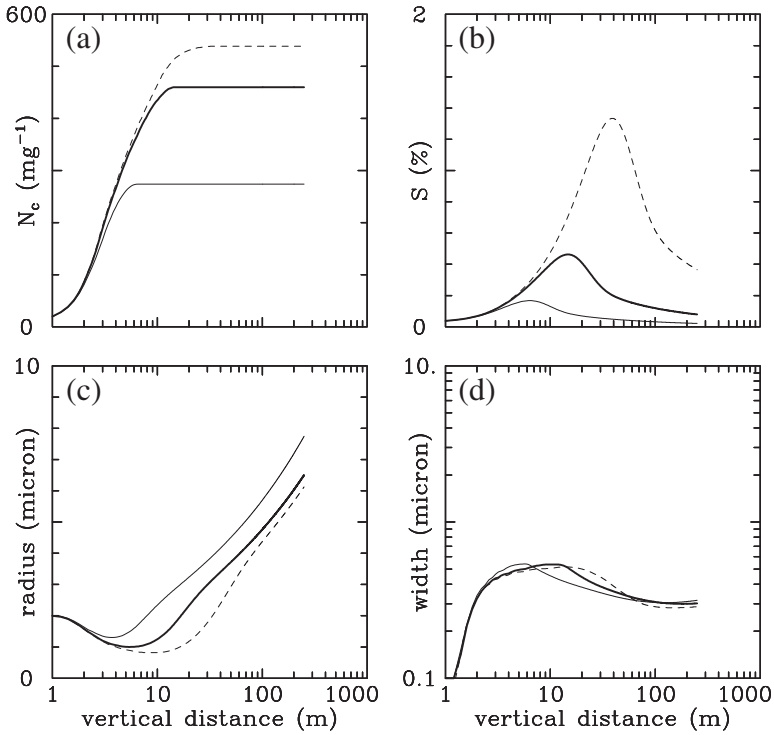

Fig. 6. As Fig. 4, but using the bin scheme described in Section 3.

w = 0.2 m s^{-1}) to about 10 m (for w = 5 m s^{-1}) above the level of zero supersaturation. This corresponds to the time delay of between 2 and 20 s. The maximum supersaturation reaches its peak deeper into the cloud for larger vertical velocity and the peak supersaturation (and thus the total concentration of activated droplets) is higher. The behavior of the droplet spectral width changes between the strong and the weak updraft. For the low vertical velocity, the width increases with time, most likely because of the evaporation (rather than growth) of some droplets (note that in this case some droplets become deactivated as shown by the decrease of the total concentration). For the strong updraft, the width starts to decrease even before the activation is completed (i.e., before S reaches its peak). The spectral widths are low, between 0.1 and 0.9 μm depending on the aerosol type and vertical velocity.

Corresponding results for the NEW scheme with $N = 300$ are shown in Figs. 6 and 7. Although the overall behavior of the solutions is similar to BNCHMK, there are some differences. First, there is no delay in the activation of first droplets because the activation starts immediately after the supersaturation becomes positive. This is also why the mean radius decreases in the first few meters as bins corresponding to progressively smaller radii are filled in. The initial trend is reversed only when a significant number of droplets is activated and they all experience some diffusional growth. The width of the droplet spectrum reaches its peak (of between 0.5 and 1 μm) before the activation is completed, and decreases thereafter. The time evolution of the spectral width only weakly depends on the updraft speed and is different than in BNCHMK. Most importantly, the number of activated droplets agrees reasonably well between BNCHMK and NEW.

Fig. 8 highlights fundamental differences between activation in the benchmark model and in the simplified bin scheme using the polluted case with $w = 1$ m s^{-1}. The figure shows the benchmark model activation time (i.e., the time when the radius of the solution droplet becomes larger than the critical radius for a given dry aerosol radius) and the supersaturation at the activation time as a function of a dry aerosol radius. Note that the critical radius in the benchmark model may be slightly different from r_{act} in Eq. (6) because the latter is obtained using a simplified formula for the quasi-equilibrium supersaturation S_{eq}. Corresponding values diagnosed applying assumptions of the simplified bin scheme are shown for comparison. The supersaturation–radius relationship in the right panel for the bin scheme is analogous to that shown in Fig. 2, except that the dry CCN radius is used instead of the solution droplet radius. For the benchmark model, activation of first droplets is delayed by about 7 s (in agreement with the results shown in Fig. 4a) and it starts with activation of CCN with dry radius of about 0.06 μm. At that moment, the supersaturation S is already around 0.3%. Subsequently, both larger and smaller CCN become activated. The larger CCN are those whose radius trails the quasi-equilibrium radius; for these S has already exceeded S_{act}. The smaller CCN are those whose radius reaches r_{act} soon after S exceeds S_{act}. Activation of large CCN continues up to the maximum S during activation (this is why the values of maximum S for small and large r in the right panel of Fig. 8 are the same), with some of the largest CCN activated even after the peak S is reached. Such a behavior is dramatically different from the simplified scheme which predicts activation of progressively smaller and smaller CCN until S reaches its peak. The difference in the activation time of the largest CCN

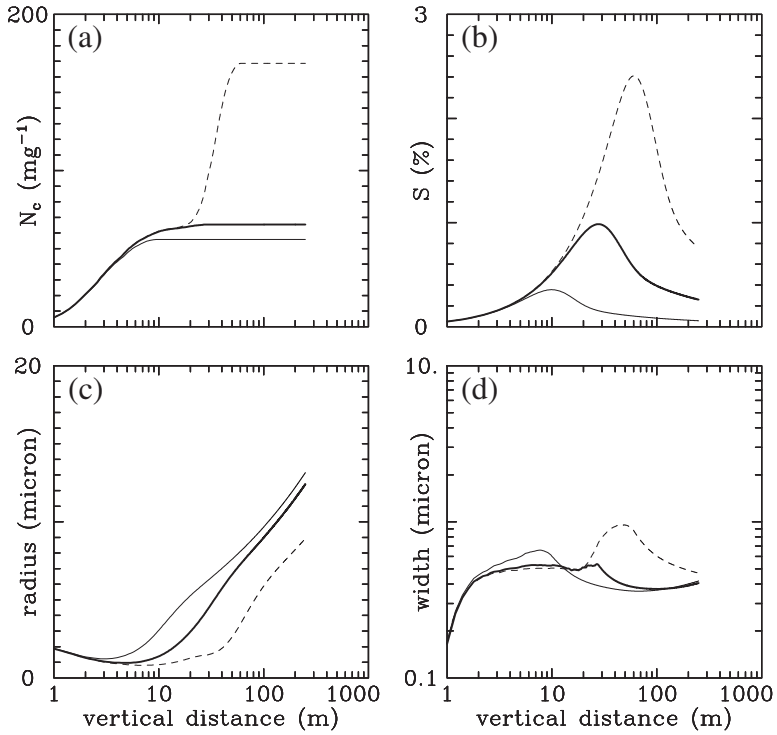

Fig. 7. As Fig. 5, but using the bin scheme described in Section 3.

is about 30 s and corresponds to about 30 m of the vertical distance. Results for $w=0.2$ and 5 m s^{-1}, as well as for the pristine aerosol, are qualitatively similar.

Table 1 summarizes results from the rising-parcel simulations from all four groups of simulations (BNCHMK, NEW, OLD, and OLD-KIN) and for the two aerosols. The table shows the concentration of activated droplets, maximum supersaturation, and the mean radius and the standard deviation of droplet spectrum at the height of 250 m above the starting level. For NEW, OLD, and OLD-KIN, the data come from simulations applying $N=112$. The only difference between results shown in the table and the $N=300$ NEW results is that

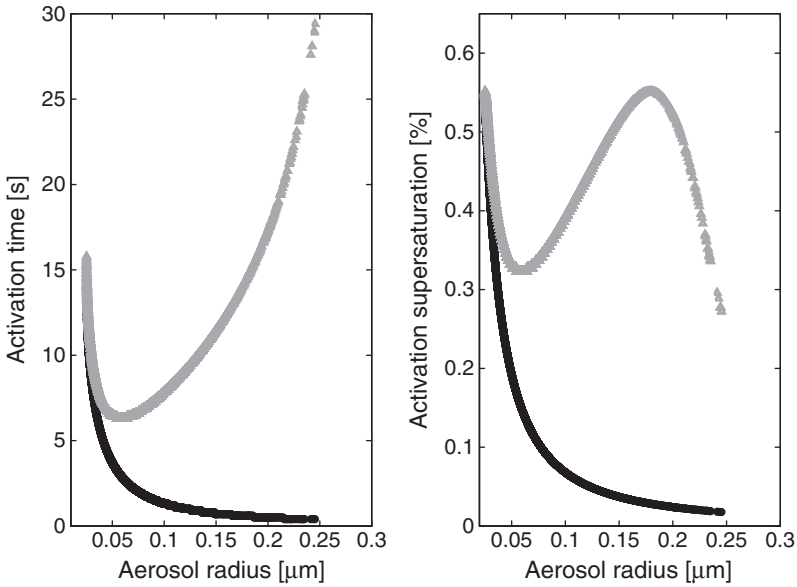

Fig. 8. Activation time (left panel) and corresponding supersaturation (right panel) as a function of the dry aerosol radius for polluted aerosol and $w=1$ m s^{-1}. Gray symbols show results from the benchmark model. Black symbols are corresponding results applying the activation representation used in the modified bin model.

Table 1
Selected results for Lagrangian rising-parcel simulations with different model setups, parcel vertical velocities, and for polluted and pristine cases with $N = 112$. The columns show the model setup (see text for explanations), vertical velocity w, concentration of activated cloud droplets N_{act}, maximum supersaturation S_{max}, and the two measures of the droplet spectrum at height of 250 m above the cloud base, the mean radius r and the standard deviation of the spectrum σ.

	w [m s^{-1}]	N_{act} [mg^{-1}]	S_{max} [%]	r [μm]	σ [μm]
Polluted					
BNCHMK	0.2	303	0.23	7.4	0.81
	1.0	482	0.55	6.4	0.36
	5.0	539	1.41	6.1	0.20
NEW	0.2	276	0.16	7.7	0.57
	1.0	464	0.46	6.5	0.51
	5.0	538	1.33	6.1	0.49
OLD	0.2	192	0.11	8.7	0.55
	1.0	366	0.26	7.0	0.47
	5.0	521	0.74	6.2	0.44
OLD-KIN	0.2	274	0.16	7.7	0.53
	1.0	447	0.42	6.5	0.48
	5.0	538	1.21	6.1	0.46
Pristine					
BNCHMK	0.2	56	0.41	13.1	0.30
	1.0	65	1.00	12.5	0.23
	5.0	168	2.42	9.0	0.47
NEW	0.2	56	0.35	13.1	0.85
	1.0	66	0.98	12.4	0.81
	5.0	171	2.39	8.9	0.66
OLD	0.2	47	0.24	13.9	0.83
	1.0	63	0.67	12.6	0.75
	5.0	124	1.78	9.9	0.63
OLD-KIN	0.2	56	0.34	13.1	0.80
	1.0	65	0.94	12.4	0.76
	5.0	164	2.26	9.0	0.61

the standard deviation for the $N = 300$ is between half and two-thirds of the values shown in the table. When rounded to the precision used in the table, all other entries for the $N = 300$ case are exactly the same. This shows that the $N = 112$ NEW setup provides satisfactory results, at least as far as the number of activated droplets and the evolution of the mean radius are concerned. For the NEW case with $N = 72$, there are some minor differences in the concentrations of activated droplets; the most significant difference is the increase of the spectral width (by about 25%) from values shown in the table. The key point is that the OLD results are significantly different from BNCHMK for both pristine and polluted aerosols: the concentration of activated droplets is significantly smaller (e.g., up to 30% in the polluted cases), so is the maximum supersaturation. Including kinetic effects improves the OLD results, but they are still not as close to BNCHMK as NEW are, especially in the polluted case (note that for the case of 5 m s^{-1} the agreement is because all available CCN become activated). The impact of various bin scheme formulations (NEW, OLD, and OLD-KIN) on the spectral width seems insignificant.

In summary, the developments presented in this paper seem to have a positive impact on the representation of activation and early growth of cloud droplets in a Twomey bin warm-rain scheme. This is despite the dramatic difference droplet activation progresses in the benchmark model and in the simplified scheme as illustrated by Fig. 8. The improved bin scheme seems to mimic the benchmark simulation relatively well, perhaps with the exception of the spectral width. Arguably, the latter is expected considering simplifications of the bin scheme, excluding the solute information in particular.

4.2. 1D Eulerian framework calculations

When the bin microphysics is used in a multidimensional cloud model, the numerical solutions of the type discussed here depend not only on the bin scheme formulation but on the spatial discretization as well. This is why it is worthwhile to test the bin scheme in a simple 1D spatial framework (e.g., Clark 1974, Morrison and Grabowski 2008). The Lagrangian adiabatic parcel framework is used to design a 1D Eulerian test with a 400-m-deep computational domain and a constant vertical velocity advecting the air across the domain. The lower ($z = 0$) boundary conditions assume constant-in-time values of the air temperature of $T = 289.16$ K and the water vapor mixing ratio selected such that the saturated conditions are reached at $z = 100$ m. The $z = 0$ pressure is assumed at 909.8 hPa which ensures that the cloud-base conditions are close to those assumed in the rising-parcel simulations. The same vertical velocities are used as before (0.2, 1 and 5 m s^{-1}) and the vertical gridlength Δz is taken as 20, 5, and 1 m in various tests. The 20 m gridlength represents a typical value for the contemporary large-eddy simulation of shallow convection, whereas the 1-m gridlength represents a possible very-high-resolution application. 1D MPDATA advection scheme of Smolarkiewicz (1984) is used to represent transport along the spatial grid. The time step (used for both the spatial advection and bin scheme) varies between 2 s for $\Delta z = 20$ m and $w = 0.2$ m s^{-1} simulations, and 0.1 s for $\Delta z = 1$ m and $w = 5$ m s^{-1} simulations. Simulations are run until the steady-state conditions are obtained.

Selected results from NEW and OLD simulations with $N = 112$ bin scheme are shown in Tables 2 and 3, together with results from BNCHMK (already shown in the Table 1), for polluted and pristine conditions, respectively. The tables include results similar to those presented in Table 1: the concentration of activated droplets, the maximum supersaturation above the cloud base, and the mean droplet radius and spectral width 250 m above the cloud base (i.e., around 50 m below the $z = 400$ m upper boundary). The results show that low vertical resolution of 20 m has significant impact on the results and leads to underpredicted/overpredicted concentrations of activated droplets for $w = 0.2/5$ m s^{-1} (the underprediction agrees with results of Clark 1974 and Morrison and Grabowski 2008). The $\Delta z = 1$ m and $\Delta z = 5$ m NEW simulations seem to mimic the BNCHMK simulations better than the OLD simulations. In particular, the OLD scheme fails to predict activation of all CCN in the $w = 5$ m s^{-1} polluted cases. An interesting aspect of the results is that the cloud droplet spectral width 250 m above the cloud base depends on the vertical gridlength: the width is significantly larger for the $\Delta z = 20$ m cases than in cases with 1 and 5-m gridlengths. Arguably, the increase of the spectral width for low vertical resolution comes from numerical diffusion during advection in the physical space of all spectral density functions $f^{(i)}$ as given by Eq. (5). This is a potentially significant result as it demonstrates that in a multidimensional Eulerian framework

Table 2
Selected results for 1D Eulerian simulations with various vertical gridlength, vertical velocities, and polluted aerosol conditions. Lagrangian model BNCHMK results are show for reference. The columns show the model setup, vertical gridlength Δz, vertical velocity w, concentration of activated cloud droplets N_{act}, maximum supersaturation S_{max}, and the mean radius r and standard deviation of the spectrum σ, both 250 m above the cloud base.

	Δz [m]	w [m s^{-1}]	N_{act} [mg^{-1}]	S_{max} [%]	r [μm]	σ [μm]
BNCHMK		0.2	303	0.23	7.4	0.81
		1.0	482	0.55	6.4	0.36
		5.0	539	1.41	6.1	0.20
NEW	20	0.2	208	0.12	8.6	1.09
	5	0.2	290	0.18	7.6	0.63
	1	0.2	270	0.17	7.7	0.57
NEW	20	1.0	457	0.42	6.6	0.90
	5	1.0	470	0.49	6.4	0.54
	1	1.0	464	0.47	6.4	0.51
NEW	20	5.0	539	1.59	6.2	0.69
	5	5.0	539	1.42	6.1	0.49
	1	5.0	539	1.33	6.1	0.49
OLD	20	0.2	143	0.09	9.8	1.01
	5	0.2	186	0.11	8.8	0.60
	1	0.2	178	0.11	8.9	0.57
OLD	20	1.0	348	0.24	7.3	0.73
	5	1.0	354	0.25	7.1	0.49
	1	1.0	357	0.26	7.0	0.47
OLD	20	5.0	539	0.92	6.3	0.55
	5	5.0	519	0.75	6.2	0.43
	1	5.0	517	0.73	6.2	0.44

the numerical solution of the bin scheme is affected not only by the bin grid resolution, but by the physical space resolution as well. The spectral width is similar in $\Delta z = 1$-m and $\Delta z = 5$-m cases which implies that the 5-m vertical gridlength or smaller results in numerical solutions that only weakly depend on the vertical resolution in the physical space. Results for $N = 300$ differ insignificantly from those shown in the tables, except for the spectral widths which are again smaller in the high-bin-resolution case, as one might anticipate based on the Lagrangian parcel simulations (cf. Table 1).

Table 3
As Table 2, but for pristine case.

	Δz [m]	w [m s^{-1}]	N_{act} [mg^{-1}]	S_{max} [%]	r [μm]	σ [μm]
BNCHMK		0.2	56	0.41	13.1	0.30
		1.0	65	1.00	12.5	0.23
		5.0	168	2.42	9.0	0.47
NEW	20	0.2	50	0.26	13.9	1.67
	5	0.2	54	0.33	13.3	0.96
	1	0.2	56	0.35	13.1	0.85
NEW	20	1.0	64	0.86	12.7	1.46
	5	1.0	65	0.98	12.4	0.86
	1	1.0	65	0.98	12.4	0.80
NEW	20	5.0	180	2.54	8.9	1.02
	5	5.0	171	2.45	8.9	0.68
	1	5.0	168	2.39	8.9	0.66
OLD	20	0.2	42	0.20	14.8	1.51
	5	0.2	45	0.22	14.2	0.91
	1	0.2	47	0.24	13.9	0.83
OLD	20	1.0	62	0.59	12.9	1.27
	5	1.0	63	0.67	12.6	0.79
	1	1.0	63	0.67	12.6	0.75
OLD	20	5.0	141	1.98	9.7	0.90
	5	5.0	124	1.82	9.9	0.64
	1	5.0	120	1.79	10.0	0.64

Table 4
Heights (m) at which radar reflectivity reaches either 0 or 20 dBz in Lagrangian rising-parcel simulations similar to those in GW09 for polluted and pristine cases, and using different number of bin ***N***. Simulation uses either the Hall gravitational kernel or Ayala turbulent kernel A100 and assume $w = 1$ m s^{-1}.

	Hall kernel		A100 kernel	
	0 dBz	20 dBz	0 dBz	20 dBz
Polluted				
$N = 400$	1952	2099	1584	1720
$N = 300$	1942	2087	1580	1715
$N = 112$	1916	2060	1584	1721
$N = 72$	1862	2014	1586	1732
Pristine				
$N = 400$	1129	1294	865	1029
$N = 300$	1123	1288	862	1026
$N = 112$	1094	1266	861	1028
$N = 72$	1064	1247	874	1048

5. Rain development in rising adiabatic parcel: GW09 revisited

Using the NEW bin microphysics setup, some of the calculations reported in GW09 were repeated. For that, the collision/coalescence representation as in GW09 was added back to the adiabatic parcel framework applied in Section 4.1. To document the impact of the improvements, Table 4 shows the heights at which the drop spectrum reaches threshold reflectivities of 0 and 20 dBz in simulations using N of 72, 112, 300 and 400 (and the bin setup as listed in Section 3.3) and applying either the Hall gravitational collision kernel or the Ayala et al. (2008a,b) kernel with the eddy dissipation rate of 100 cm^2 s^{-3} (A100); see GW09 for details.

As in GW09, increasing the number of bins N results in the delayed rain development for the Hall gravitational kernel. However, the differences in heights at which reflectivities of 0 and 20 dBz are reached for various bin grid setups are significantly smaller than in GW09, tens of meters in most cases instead of hundreds of meters in GW09. For the A100 kernel, the changes are more complicated and most likely not statistically significant. This is because the height changes of a few meters (compared to the entries in the table) are observed in simulations that apply different time steps for the same N (not shown). This also suggests that results for $N = 300$ and 400 are close to the numerically converged solutions. Since solutions for $N = 112$, or even $N = 72$, are relatively close to the $N = 300$ solutions—especially when compared to the differences in GW09—such bin resolutions might be considered for the multidimensional Eulerian framework.

6. Summary

This paper presents improvements to the bin microphysics representation of cloud droplet activation and diffusional growth that ultimately allow obtaining converged numerical solutions of the rain formation in numerical models of clouds. Simplified treatment of these processes in Grabowski and

Wang (2009; GW09) made the latter impossible. The emphasis here is on the representation of droplet activation using a simple representation of CCN characteristics that uniquely relates the concentration of activated droplets N_{CCN} to the supersaturation S experienced by the air parcel. The $N_{CCN}-S$ relationship is often referred to as the Twomey relationship (Twomey 1959) and is typically expressed as $N_{CCN}=C_0\ (100S)^k$, where C_0 and k are coefficients based on the observed CCN characteristics. Such a bulk description is used in some cloud models because it allows representing in a simple way the effects of CCN on cloud droplet spectra, for instance, the differences between clouds developing in clean and polluted environments. The key aspect is that such an approach excludes complications of CCN size distribution and chemical composition that is used in more complicated (and consequently more computational intensive) approaches (see the Introduction). Moreover, the Twomey relationship is typically used in such a way that the freshly activated droplets are inserted into the first radius bin of spectral representation (e.g., Clark 1974; Hall 1980; Grabowski 1989; Stevens et al. 1996; Rasmussen et al. 2002). All these simplifications can potentially affect growth of small cloud droplets and thus feed back on the details of CCN activation.

The approach used in this paper is to compare results from an accurate benchmark Lagrangian scheme (tracing growth of 10,000 solution droplets from the prescribed initial distribution of CCN) with a standard bin microphysics scheme (i.e., using the spectral density function) applying the Twomey approach to represent droplet activation. With relatively straightforward modifications of the bin microphysics scheme, the scheme is capable in reproducing the benchmark solutions (with the exception of the spectral width). The modifications of the bin microphysics include: (i) improved activation scheme (with a simple procedure to insert activated CCN into size bins corresponding to progressively smaller radii when the supersaturation increases near the cloud base); (ii) updated droplet growth equation (including the kinetic effects but omitting the curvature and solute effects); (iii) extending the bin grid into sub-micron radii; and (iv) applying a more accurate Lagrangian approach to calculate the shift of the spectral density function due to diffusional growth. Results from a large number of numerical tests compiled during the course of this study, including both parcel simulations as well as 1D Eulerian updraft simulations, suggest that all these modifications play role in the overall improvement of the bin scheme.

The tests reported here suggest the bin and spatial resolutions that should be used in large-eddy simulations to address with confidence the impact of cloud turbulence on drizzle/rain development in warm clouds given the numerical techniques applied here to represent processes in the radius space and in the physical space. For the bin grid, $N=112$ (or maybe even $N=72$) appears to be a sensible compromise between accuracy and computational cost. The resolution in the physical space in 1D Eulerian tests was shown here not only to impact the concentration of activated droplets (in agreement with previous studies of Clark 1974 and Morrison and Grabowski 2008) but also the width of cloud droplet spectrum a few hundred meters above the cloud base. Because numerical widening of the droplet spectrum affects the development of rain through collision/coalescence, sufficiently high spatial resolution needs to be used. In Eulerian tests, a vertical gridlength of $\Delta z=5$ m seems to produce solution close to those that might be considered numerically converged and at least such a spatial resolution should ultimately be used. One has to keep in mind, however, that the above conclusions apply only to a specific bin and activation schemes used here and should be extrapolated to different bin schemes with caution. Large-eddy simulations with bin and spatial resolutions recommended here are currently underway and their results will be reported in forthcoming publications.

Acknowledgments

Part of this work was completed during WWG visit to the French National Center for Meteorological Research (CNRM), Toulouse, supported by the CNRM's Research Visitor Fellowship. This material is based upon work supported by the National Science Foundation under award number OCI-0904449 (PetaApps). WWG was also partially supported by the NOAA grant NA08OAR4310543i and DOE ARM grant DE-FG02-08ER64574. MA acknowledges the award of NERC funding for the VOCALS project, NCAS-supported computer time on HECToR, and use of BADC data centre. LPW acknowledges the support from NSF through grants ATM-0527140 and ATM-0730766. Comments on the manuscript by Yefim Kogan, Hugh Morrison, and two anonymous reviewers are acknowledged. The National Center for Atmospheric Research is operated by the University Corporation for Atmospheric Research under sponsorship of the National Science Foundation.

Appendix. Details of the benchmark model

The benchmark model is a 1D version of the model described in Andrejczuk et al. (2008). It assumes that CCN are ammonium sulfate and solves Eq. (2) with the equilibrium supersaturation defined as:

$$S_{eq}=\exp\left(\frac{2\sigma}{R_v\rho_w Tr}-\frac{\nu\Phi m_a M_w/M_s}{4/3\pi\rho_w\left(r^3-r_a^3\right)}\right)-1, \tag{10}$$

where M_w is the molecular weight of water; M_s is the molecular weight of ammonium sulfate; σ is the surface tension of water; ν is the van't Hoff factor; Φ is the molar osmotic coefficient of ammonium sulfate ($\nu\Phi=2$); and r_a and m_a are the radius and mass of the dry aerosol particle. Diffusion coefficient of water vapor and thermal conductivity of air are taken in the benchmark model as $D'=(0.015T-1.9)\times10^{-5}$ m^2 s^{-1} and $K'=1.5\times10^{-11}T^3-4.8\times10^{-8}T^2+1.0\times10^{-4}T-3.9\times10^{-4}$ W m^{-1} K^{-1}. Both diffusion coefficient and thermal conductivity were modified to take into account the kinetic effects (Pruppacher and Klett 1997, Ch. 13):

$$D=D'\left[\frac{r}{r+\Delta_v}+\frac{D'}{r\alpha_c}\left(\frac{2\pi}{R_vT}\right)^{\frac{1}{2}}\right]^{-1} \tag{11a}$$

$$K=K'\left[\frac{r}{r+\Delta_T}+\frac{K'}{r\alpha_T\rho_o c_p}\left(\frac{2\pi}{R_dT}\right)^{\frac{1}{2}}\right]^{-1} \tag{11b}$$

Table 5
Parameters used to prescribe the two modes of the aerosol distributions. See Andrejczuk et al. (2008) for details.

	N_1 [cm^{-3}]	r_1 [μm]	σ_1 [1]	N_2 [cm^{-3}]	r_2 [μm]	σ_2 [1]
Polluted	160	0.029	1.36	380	0.071	1.57
Pristine	125	0.011	1.20	65	0.060	1.70

where α_c/α_T are the condensation/thermal accommodation coefficients; Δ_v/Δ_T are the "vapor/thermal jump" lengths; R_d is the dry-air gas constant; ρ_o is the air density; and c_p is the specific heat of air at constant pressure. Constants listed in Pruppacher and Klett (1997; Table 13-1) are used to calculate kinetic corrections for D and K.

The benchmark model traces growth of 10,000 solution droplets with dry radii randomly selected from a prescribed CCN size distribution. A two-modal lognormal distribution is used for both polluted VOCALS and pristine DYCOMS cases with parameters for each case listed in Table 5. Rosenbrock method (Press et al. 1992) is applied to advance Eq. (2) in time for each solution droplet using a variable time step, with the tolerance and the initial time step of 10^{-3} and 10^{-6} s, respectively. The solution is saved every 0.1 s. At the start of Lagrangian calculations, Eq. (2) is used for each aerosol particle with $S=0$ (i.e., saturated conditions) for 3 min so each solution droplet reaches the equilibrium radius.

References

Ackerman, A.S., Toon, O.B., Hobbs, P.V., 1995. A model for particle microphysics, turbulent mixing, and radiative transfer in the stratocumulus-topped marine boundary layer and comparisons with measurements. J. Atmos. Sci. 52, 1204–1236.

Ackerman, A.S., Coauthors, 2009. Large-eddy simulations of a drizzling stratocumulus-topped marine boundary layer. Mon. Wea. Rev. 137, 1083–1110.

Andrejczuk, M., Reisner, J.M., Henson, B., Dubey, M.K., Jeffery, C.A., 2008. The potential impacts of pollution on a nondrizzling stratus deck: does aerosol number matter more than type? J. Geophys. Res. 113, D19204. doi:10.1029/2007JD009445.

Ayala, O., Rosa, B., Wang, L.-P., Grabowski, W.W., 2008a. Effects of turbulence on the geometric collision rate of sedimenting droplets: Part 1. Results from direct numerical simulation. New J. Phys. 10, 075015. doi:10.1088/1367-2630/10/7/075015.

Ayala, A., Rosa, B., Wang, L.-P., 2008b. Effects of turbulence on the geometric collision rate of sedimenting droplets: Part 2. Theory and parameterization. New J. Phys. 10, 075016. doi:10.1088/1367-2630/10/7/075016.

Bott, A., 2000. A flux method for the numerical solution of the stochastic collection equation: extension to two-dimensional particle distributions. J. Atmos. Sci. 57, 284–294.

Clark, T.L., 1973. Numerical modeling of the dynamics and microphysics of warm cumulus convection. J. Atmos. Sci. 30, 857–878.

Clark, T.L., 1974. On modelling nucleation and condensation theory in Eulerian spatial domain. J. Atmos. Sci. 31, 2099–2117.

Feingold, G., Tzivion, S., Levin, Z., 1988. Evolution of raindrop spectra. Part I: solution to the stochastic collection/breakup equation using the method of moments. J. Atmos. Sci. 45, 3387–3399.

Feingold, G., Stevens, B., Cotton, W.R., Walko, R.L., 1994. An explicit cloud microphysics/LES model designed to simulate the Twomey effect. Atmos. Res. 33, 207–233.

Fukuta, N., Walter, L.A., 1970. Kinetics of hydrometeor growth from a vapor-spherical model. J. Atmos. Sci. 27, 1160–1172.

Grabowski, W.W., 1989. Numerical experiments on the dynamics of the cloud–environment interface: small cumulus in a shear-free environment. J. Atmos. Sci. 46, 3513–3541.

Grabowski, W.W., Wang, L.-P., 2009. Diffusional and accretional growth of water drops in a rising adiabatic parcel: effects of the turbulent collision kernel. Atmos. Chem. Phys. 9, 2335–2353.

Grabowski, W.W., Thouron, O., Pinty, J.-P., Brenguier, J.-L., 2010. A hybrid bulk-bin approach to model warm-rain processes. J. Atmos. Sci. 67, 385–399.

Hall, W.D., 1980. A detailed microphysical model within a two-dimensional framework: model description and preliminary results. J. Atmos. Sci. 37, 2486–2507.

Howell, W.E., 1949. The growth of cloud drops in uniformly cooled air. J. Atmos. Sci. 6, 134–149.

Khain, A.P., Ovtchinnikov, M., Pinsky, M., Pokrovsky, A., Krugliak, H., 2000. Notes on the state-of-the-art numerical modeling of cloud microphysics. Atmos. Res. 55, 159–224.

Khain, A., Pokrovsky, A., Pinsky, M., Seifert, A., Phillips, V., 2004. Effects of atmospheric aerosols on deep convective clouds as seen from simulations using a spectral microphysics mixed-phase cumulus cloud model Part 1: model description. J. Atmos. Sci. 61, 2963–2982.

Kogan, Y.L., 1991. The simulation of a convective cloud in a 3-D model with explicit microphysics. Part I: model description and sensitivity experiments. J. Atmos. Sci. 48, 1160–1189.

Leroy, D., Wobrock, W., Flossmann, A.I., 2007. On the influence of the treatment of aerosol particles in different bin microphysical models: a comparison between two different schemes. Atmos. Res. 85, 269–287.

Morrison, H., Grabowski, W.W., 2007. Comparison of bulk and bin warm rain microphysics models using a kinematic framework. J. Atmos. Sci. 64, 2839–2861.

Morrison, H., Grabowski, W.W., 2008. Modeling supersaturation and subgrid-scale mixing with two-moment bulk warm microphysics. J. Atmos. Sci. 65, 792–812.

Press, W., Teukolsky, S., Vetterling, W.T., Flannery, B.P., 1992. Numerical Recipes in Fortran 77: The Art of Scientific Computing. Cambridge Univ. Press.

Pruppacher, H.R., Klett, J.D., 1997. Microphysics of Clouds and Precipitation. Kluwer Academic.

Rasmussen, R.M., Geresdi, I., Thompson, G., Manning, K., Karplus, E., 2002. Freezing drizzle formation in stably stratified layer clouds: the role of radiative cooling of cloud droplets, cloud condensation nuclei, and ice initiation. J. Atmos. Sci. 59, 837–860.

Reisin, T., Levin, Z., Tzvion, S., 1996. Rain production in convective clouds as simulated in an axisymmetric model with detailed microphysics. Part 1: description of the model. J. Atmos. Sci. 53, 497–519.

Simmel, M., Wurzler, S., 2006. Condensation and activation in sectional cloud microphysical models. Atmos. Res. 80, 218–236.

Smolarkiewicz, P.K., 1984. A fully multidimensional positive definite advection transport algorithm with small implicit diffusion. J. Comput. Phys. 54, 325–362.

Srivastava, R.C., 1991. Growth of cloud drops by condensation: effect of surface tension on the dispersion of drop sizes. J. Atmos. Sci. 48, 1596–1605.

Stevens, B., Feingold, G., Cotton, W.R., Walko, R.L., 1996. Elements of the microphysical structure of numerically simulated nonprecipitating stratocumulus. J. Atmos. Sci. 53, 980–1006.

Twomey, S., 1959. The nuclei of natural cloud formation part II: the supersaturation in natural clouds and the variation of cloud droplet concentration. Pure Appl. Geophys. 43, 243–249.